A Lattice Dynamical Investigation of the Raman and the Infrared Wave Numbers of $MnWO_4$

H.C. Gupta[a], Ruby[b] and M.M. Sinha[b,*]
[a]Department of Physics, Indian Institute of Technology, Delhi, Hauz Khas, New Delhi-110016, India
[b]Department of Physics, Sant Longowal Institute of Engineering and Technology, Longowal, Sangrur-148106, India

(Received December 15, 2011; in final form February 20, 2012)

A short-range force constant model has been applied using normal coordinate analysis to investigate the Raman and the infrared modes in multiferroic $MnWO_4$ having space group $P2/c$. The calculation of zone centre phonons has been made with eight stretching and seven bending force constants. The calculated Raman and infrared wave numbers are in good agreement with the observed ones. The potential energy distribution has also been investigated for determining the significance of contribution from each force constant toward the Raman and the infrared wave numbers.

PACS: 61.50.Ah, 63.22.Dc, 63.70.+h, 75.10.Pq, 78.30.−j

1. Introduction

Multiferroic materials have recently attracted much attention due to their unique magnetic and electric properties, i.e., coexistence of spontaneous polarization and magnetization in the same phase. Simple tungstate $MnWO_4$ is one of the well known magnetoelectric multiferroics in which ferroelectricity is induced through the non-collinear spin structure at low temperatures [1–3].

One of the advantages of studying $MnWO_4$ is that it has only one kind of magnetic ion (Mn^{2+}) whereas other multiferroic oxides usually have multiple magnetic ions, thus hindering investigation of their magnetic properties. With the advantage of single magnetic ion, we are provided with a clear window into the electromagnetic coupling behaviour and are able to make simple analyses of the magnetic field dependence and spin–orbit coupling effects.

$MnWO_4$ has also been found a prospective material for application as a humidity sensor and efficient catalyst for organic dye photodegradation in sunlight [4–6].

The magnetic phases of $MnWO_4$ are characterized by various antiferromagnetic (AF) states such that the first antiferromagnetic phase appears below $T_{N3} \approx 13.5$ K. Successive magnetic phase transitions occur at $T_{N2} \approx 12.5$ K and $T_{N1} \approx 6.5$–8 K, forming three different antiferromagnetically ordered phases: AF1 ($T \leq T_{N1}$), AF2 ($T_{N1} \leq T \leq T_{N2}$), and AF3 ($T_{N2} \leq T \leq T_{N3}$). These magnetic phases have been characterized by neutron-scattering experiments, which have shown that AF1 has a collinear up-up-down–down spin structure, AF2 has a noncollinear spiral spin structure, and AF3 has a sinusoidal collinear spin structure [7, 8]. Spontaneous electric polarization occurs at AF2, which suggests that the noncollinear spiral structure might be the origin of the induced ferroelectricity in $MnWO_4$. The appearance of ferroelectricity in AF2 phase indicates the spin lattice coupling and hence the investigation of phonons is very much important. Therefore, many attempts have been made to study the Raman and infrared phonons experimentally [9–12]. As per our knowledge, first of all Iliev et al. [9] had calculated Raman phonon frequencies by using shell model but the infrared phonon frequencies have not been reported by them. Choi et al. [12] observed the infrared (TO) phonons for three different polarisation directions by conducting the Kramers–Kronig analysis and reflectance spectra but no assignment was proposed for these infrared phonons. Maczka et al. [10] predicted the Raman and infrared phonons for $MnWO_4$ with small amount of doping of Fe and Co on the basis of four-parameter model. They have also calculated wave numbers for doped $MnWO_4$ with the help of ionic shell model. Hence in this paper an attempt has been made to study the Raman and infrared phonons of pure form of $MnWO_4$ by using the short range force constant model for the first time in $P2/c$ structure. For the study of zone centre phonons, 8 stretching and 7 bending force constants have been used. There is a very good agreement between the theoretical calculated values and the experimental values.

Further, our theoretically calculated values approach more closer to experimental ones than the values reported by Iliev et al. [9]. The contribution from each force constant towards the Raman and the infrared wave numbers is also determined with the help of potential energy distribution (PED).

2. Structure

$MnWO_4$ has wolframite crystal structure which belongs to group of tungstates, containing WO_6 octahedra [11, 13]. $MnWO_4$ crystallizes in a monoclinic structure (space group symmetry $P2/c = 13\text{-}C_{2h}$). The primitive cell contains two formula units i.e. contains 12 atoms in a unit cell. The structure is shown in Fig. 1. The lattice parameters are $a = 4.830(1)$ Å, $b = 5.7603(9)$ Å,

* corresponding author; e-mail: mm_sinha@rediffmail.com

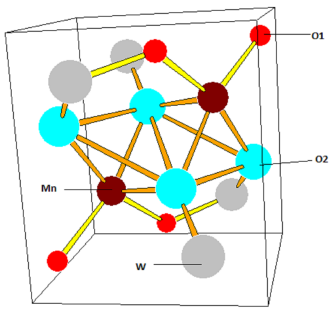

Fig. 1. Crystal structure of $MnWO_4$.

$c = 4.994(1)$ Å, $\beta = 91.14(2)0$, $V = 138.8(1)$ Å^3 and $Z = 2$ [14]. Table I represents the site symmetry, atomic coordinates [14] and the phonon contribution at the Γ point.

The total number of zone centre phonon modes present for each species of space group is

$$\Gamma_{\text{total}} = 8A_{\text{g}} + 10B_{\text{g}} + 8A_{\text{u}} + 10B_{\text{u}}.$$

Out of these $1A_{\text{u}} + 2B_{\text{u}}$ are acoustical modes. So the active optical modes are given as

$$\Gamma_{\text{optical}} = 8A_{\text{g}} + 10B_{\text{g}} + 7A_{\text{u}} + 8B_{\text{u}}.$$

Further $8A_{\text{g}}, 10B_{\text{g}}$ are Raman active and $7A_{\text{u}}$, $8B_{\text{u}}$ are infrared active modes.

TABLE I

Site symmetry, atomic coordinates for $MnWO_4$, and phonon contribution at Γ point.

Atoms	Sites	X	Y	Z	Phonon contribution at point
Mn	2f	0.500	0.6856	0.250	$A_{\text{g}} + 2B_{\text{g}} + A_{\text{u}} + 2B_{\text{u}}$
W	2e	0.000	0.1800	0.250	$A_{\text{g}} + 2B_{\text{g}} + A_{\text{u}} + 2B_{\text{u}}$
O1	4g	0.211	0.1020	0.943	$3A_{\text{g}} + 3B_{\text{g}} + 3A_{\text{u}} + 3B_{\text{u}}$
O2	4g	0.250	0.3740	0.3933	$3A_{\text{g}} + 3B_{\text{g}} + 3A_{\text{u}} + 3B_{\text{u}}$

TABLE II

Symmetry coordinates of $MnWO_4$ in $P2/c$ structure.

Species	S. No.	Symmetry coordinates	Species	S. No.	Symmetry coordinates
A_{g}			A_{u}		
	1	$(Mn_{1y}$ - $Mn_{2y})/\sqrt{2}$		19	$(Mn_{1y}+ Mn_{2y})/\sqrt{2}$
	2	$(W_{1y}$ - $W_{2y})/\sqrt{2}$		20	$(W_{1y} + W_{2y})/\sqrt{2}$
	3	$(O1_{1X}$ - $O1_{2X}$ - $O1_{3X} + O1_{4X})/2$		21	$(O1_{1X}$ - $O1_{2X} + O1_{3X}$ - $O1_{4X})/2$
	4	$(O1_{1Y} + O1_{2Y}$ - $O1_{3Y}$ - $O1_{4Y})/2$		22	$(O1_{1Y} + O1_{2Y} + O1_{3Y} + O1_{4Y})/2$
	5	$(O1_{1Z}$ - $O1_{2Z}$ - $O1_{3Z} + O1_{4Z})/2$		23	$(O1_{1Z}$ - $O1_{2Z} + O1_{3Z}$ - $O1_{4Z})/2$
	6	$(O2_{1X}$ - $O2_{2X}$ - $O2_{3X} + O2_{4X})/2$		24	$(O2_{1X}$ - $O2_{2X} + O2_{3X}$ - $O2_{4X})/2$
	7	$(O2_{1Y} + O2_{2Y}$ - $O2_{3Y}$ - $O2_{4Y})/2$		25	$(O2_{1Y} + O2_{2Y} + O2_{3Y} + O2_{4Y})/2$
	8	$(O2_{1Z}$ - $O2_{2Z}$ - $O2_{3Z} + O2_{4Z})/2$		26	$(O2_{1Z}$ - $O2_{2Z} + O2_{3Z}$ - $O2_{4Z})/2$
B_{g}			B_{u}		
	9	$(Mn_{1X}$ - $Mn_{2X})/\sqrt{2}$		27	$(Mn_{1X} + Mn_{2X})/\sqrt{2}$
	10	$(Mn_{1Z}$ - $Mn_{2Z})/\sqrt{2}$		28	$(Mn_{1Z} + Mn_{2Z})/\sqrt{2}$
	11	$(W_{1X}$ - $W_{2X})/\sqrt{2}$		29	$(W_{1X} + W_{2X})/\sqrt{2}$
	12	$(W_{1Z}$ - $W_{2Z})/\sqrt{2}$		30	$(W_{1Z} + W_{2Z})/\sqrt{2}$
	13	$(O1_{1X} + O1_{2X}$ - $O1_{3X}$ - $O1_{4X})/2$		31	$(O1_{1X} + O1_{2X} + O1_{3X}+O1_{4X})/2$
	14	$(O1_{1Y}$ - $O1_{2Y}$ - $O1_{3Y} + O1_{4Y})/2$		32	$(O1_{1Y}$ - $O1_{2Y}+O1_{3Y}$ - $O1_{4Y})/2$
	15	$(O1_{1Z} + O1_{2Z}$ - $O1_{3Z}$ - $O1_{4Z})/2$		33	$(O1_{1Z} + O1_{2Z} + O1_{3Z} + O1_{4Z})/2$
	16	$(O2_{1X} + O2_{2X}$ - $O2_{3X}$ - $O2_{4X})/2$		34	$(O2_{1X}+O2_{2X} + O2_{3X} + O2_{4X})/2$
	17	$(O2_{1Y}$ - $O2_{2Y}$ - $O2_{3Y} + O2_{4Y})/2$		35	$(O2_{1Y}$ - $O2_{2Y}+ O2_{3Y}$ - $O2_{4Y})/2$
	18	$(O2_{1Z} + O2_{2Z}$ - $O2_{3Z}$ - $O2_{4Z})/2$		36	$(O2_{1Z} + O2_{2Z} + O2_{3Z} +O2_{4Z})/2$

3. Theory

The present normal coordinate analysis is based on the Wilson–GF matrix method and makes use of Cartesian symmetry coordinates [15]. The eigenvalue equation is given by

$$|FG - E\lambda| = 0,$$

where F is a matrix of force constants and thus brings the potential energies of vibrations into the equation, G is a matrix that involves the masses and certain spatial relationships of the atoms and thus brings the kinetic

energies into the equation, E is a unit matrix and λ which brings the frequency ν into the equation is defined by:

$\lambda = 4\pi^2 c^2 \nu^2$.

The matrix F was constructed by using short-range force constant model (SRFCM). The short-range forces are the forces that are effective up to certain neighbours only. Their magnitude diminishes generally after the second-neighbour inter-atomic interactions. The stretching forces between two atoms were assumed to be obeying the Hooke law. The stretching forces alone are not adequate to account for transverse vibrations in the lattice and therefore bending forces were included in the calculation. In this model bending forces are considered to arise from the resistance to the deformation of the angles of the triangles formed by atoms with its two neighbours. To evaluate the changes in the angles of a triangle, a comparison is made between the triangle in the equilibrium position and the projection of the deformed triangle onto the equilibrium plane.

TABLE III

Interatomic force constant values for $MnWO_4$.

Force constant	Between atoms	Coordination number	Interatomic distance [Å]/angle*	Force constant values [N/cm]
K_1	W–O2	4	1.784	3.701
K_2	W–O1	4	1.911	2.196
K_3	Mn–O1	4	2.104	1.283
K_4	W–O1	4	2.137	1.224
K_5	Mn–O2	4	2.161	0.421
K_6	Mn–O2	4	2.285	0.252
K_7	O2–O2	2	2.781	0.131
K_8	W–Mn	4	3.734	2.314
H_1	O1–Mn–O2	4	87.88	0.065
H_2	O1–Mn–O2	4	95.71	0.284
H_3	O1–W–O2	4	96.16	0.120
H_4	O1-W–Mn	4	27.36	0.335
H_5	O2–W–Mn	4	156.26	0.123
H_6	W–O1–W	4	106.63	1.405
H_7	Mn–W–O1	4	61.37	0.290

* Angles are in degrees.

Potential energy includes short range stretching forces between W–O2, W–O1, Mn–O1, Mn–O2, O2–O2, W–Mn, atoms and bending forces between O1–Mn–O2, O1–W–O2, O1–W–Mn, O2–W–Mn, W–O1–W and Mn–W–O1 atoms only. The input parameters used for the calculation are the lattice parameter, mass of the atoms, and symmetry coordinates. The symmetry coordinates for the Raman and the infrared modes at zone centre are given in Table II, for the first time in monoclinic $P2/c$ structure. The short-range force constants are optimized to give the best fit of the observed Raman and infrared wave numbers. These inter-atomic force constants so obtained are presented in Table III.

4. Results and discussion

In this work we have calculated the Raman as well as the infrared modes using the force constants given in Table III. These values are compared with the experimentally determined Raman modes by Iliev et al. [9] and infrared modes by Maczka et al. [10] in Table IV. It is obvious from Table IV that there is a good agreement between the theory and the experiment for both Raman and infrared modes, establishing the present calculations. The potential energy distributions for each mode are investigated to determine the contribution of different force constants to various frequencies. The interpretations drawn from the PED are described below.

The force constant W–O1–W contributes in dominant way for the high frequency mode i.e. 839 cm^{-1} of A_g mode, 846 cm^{-1} of B_g mode, 845 cm^{-1} of A_u mode, 885 cm^{-1} of B_u mode. For frequencies 694 cm^{-1} of A_g, 695 cm^{-1} of B_g, 695 cm^{-1} of A_u and 695 cm^{-1} of B_u, W–O2 force constant plays an important role. From theoretical calculations, W–O1 force constant were found as leading force constant for frequencies 519 cm^{-1} of A_g, 539 cm^{-1} of B_g, 529 cm^{-1} of A_u and 533 cm^{-1} of B_u. For frequencies 392 cm^{-1} of A_g, 380 cm^{-1} of B_g, 406 cm^{-1} of A_u and 411 cm^{-1} of B_u, force constant W–Mn is of utmost significance. It is important to mention that an important W–Mn bond, when not considered, the lowest frequency of B_g was obtained very small as compared to the experimental value. Force constant O1–W–O2 plays a vital role for lower frequencies 148 cm^{-1} of A_g, 94 cm^{-1} of B_g, 157 cm^{-1} of A_u and 123 cm^{-1} of B_u.

It is important to mention that the shell model uses more number of parameters than the present short-range force constant model. Also, the overall agreement obtained in the present calculations with the experiment is better than the shell model calculations. It is important to note that the present calculated values in the range (400–500 cm^{-1}) are in close agreement with the experiment when compared with the calculated values due to Iliev et al. [9].

References

[1] O. Heyer, N. Hollmann, I. Klassen, S. Jodlauk, L. Bohaty, P. Becker, J.A. Mydosh, T. Lorenz, D. Khomskii, *J. Phys., Condens. Matter* **18**, L471 (2006).

[2] K. Taniguchi, N. Abe, H. Sagayama, S. Otani, T. Takenobu, Y. Iwasa, T. Arima, *Phys. Rev. B* **77**, 064408 (2008).

[3] A.H. Arkenbout, T.T.M. Palstra, T. Siegrist, T. Kimura, *Phys. Rev. B* **74**, 184431 (2006).

[4] L. Zhang, C. Lu, Y. Wang, Y. Cheng, *Mater. Chem. Phys.* **103**, 433 (2007).

[5] J. Maier, *Solid State Ionics* **175**, 7 (2004).

[6] H.Y. He, J.F. Huang, L.Y. Cao, J.P. Wu, *Desalination* **252**, 66 (2010).

[7] G. Lautenschläger, H. Weitzel, T. Vogt, R. Hock, A. Boehm, M. Bonnet, H. Fuess, *Phys. Rev. B* **48**, 6087 (1993).

[8] H. Ehrenberg, H. Weitzel, H. Fuess, B. Hennion, *J. Phys., Condens. Matter* **11**, 2649 (1999).

[9] M.N. Iliev, M.M. Gospodinov, A.P. Litvinchuk, *Phys. Rev. B* **80**, 212302 (2009).

TABLE IV

Calculated and observed Raman and infrared active zone centre modes (in cm^{-1}) for $MnWO_4$.

Species	Observed wave numbers	Present calculated wave numbers	Calculated wave numbers by Iliev et al. [9] and Maczka et al. [10]	Two dominant contributions as per PED
$A_{g,1}$	129	148	125	H_3 — 34%, H_1 — 20%
$A_{g,2}$	206	183	195	H_6 — 39%, K_3 — 22%
$A_{g,3}$	258	269	280	H_7 — 30%, K_5 — 20%
$A_{g,4}$	327	317	330	H_2 — 23%, H_7 — 14%
$A_{g,5}$	397	392	453	K_8 — 61%, H_7 — 14%
$A_{g,6}$	545	519	551	K_2 — 43%, K_4 — 34%
$A_{g,7}$	698	694	639	K_1 — 85%, H_2 — 3%
$A_{g,8}$	885	839	830	H_6 — 54%, K_3 — 20%
$B_{g,1}$	89	94	123	H_3 — 38%, K_6 — 21%
$B_{g,2}$	160	131	150	H_2 — 19%, K_5 — 18%
$B_{g,3}$	166	190	173	K_4 — 22%, H_6 — 16%
$B_{g,4}$	177	211	248	K_4 — 19%, H_1 — 16%
$B_{g,5}$	272	298	309	K_5 — 29%, H_5 — 21%
$B_{g,6}$	294	334	334	H_7 — 20%, H_5 — 17%
$B_{g,7}$	356	380	406	K_8 — 38%, H_2 — 28%
$B_{g,8}$	512	539	482	K_2 — 49%, K_4 — 31%
$B_{g,9}$	674	695	674	K_1 — 88%, H_2 — 4%
$B_{g,10}$	774	846	758	H_6 — 51%, K_3 — 21%
A_{u1}	0.0	0.0	0.0	
A_{u2}	182	157	156	H_3 — 32%, H_1 — 28%
A_{u3}	307	262	246	H_7 — 23%, H_5 — 22%
A_{u4}	348	319	410	H_2 — 29%, H_7 — 23%
A_{u5}	420	406	455	K_8 — 58%, K_3 — 14%
A_{u6}	495	529	547	K_2 — 44%, K_4 — 35%
A_{u7}	656	695	671	K_1 — 84%, H_2 — 4%
A_{u8}	861	845	837	H_6 — 54%, K_3 — 19%
B_{u1}	0.0	0.0	0.0	
B_{u2}	0.0	0.0	0.0	
B_{u3}	152	123	163	H_3 — 47%, H_1 — 32%
B_{u4}	248	223	206	H_5 — 24%, H_7 — 36%
B_{u5}	280	279	263	K_5 — 47%, H_5 — 16%
B_{u6}	324	333	323	H_7 — 26%, H_2 — 25%
B_{u7}	...	411	467	K_8 — 43%, K_3 — 18%
B_{u8}	577	533	576	K_2 — 42%, K_4 — 36%
B_{u9}	739	695	...	K_1 — 85%, H_2 — 5%
B_{u10}	885	885	...	H_6 — 53%, K_3 — 17%

[10] M. Maczka, M. Ptak, K. Hermanowicz, A. Majchrowski, A. Pikul, J. Hanuza, *Phys. Rev. B* **83**, 174439 (2011).

[11] L.H. Hoang, N.T.M. Hien, W.S. Choi, Y.S. Lee, K. Taniguichi, T. Arima, S. Yoon, X.B. Chen, In-Sang Yang, *J. Raman Spectrosc.* **41**, 1005 (2010).

[12] W.S. Choi, K. Taniguchi, S.J. Moon, S.S.A. Seo, T. Arima, H., Hoang, I.S. Yang, T.W. Noh, Y.S. Lee, *Phys. Rev. B* **81**, 205111 (2010).

[13] K. Taniguchi, N. Abe, T. Takenobu, Y. Iwasa, T. Arima, *Phys. Rev. Lett.* **97**, 097203 (2006).

[14] J. Macavei, H. Schulz, *Z. Kristallogr.* **207**, 193 (1993).

[15] T. Shimanouchi, M. Tsuiboi, T. Miyawaza, *J. Chem. Phys.* **35**, 1597 (1961).